



**UNICA**

UNIVERSITÀ  
DEGLI STUDI  
DI CAGLIARI



Università di Cagliari

**UNICA IRIS Institutional Research Information System**

**This is the Author's submitted manuscript version of the following contribution:**

Mura M., Carucci C., Cesare Marincola F., Monduzzi M., Parsons D.F., Salis A. The melting curves of calf thymus-DNA are buffer specific, *Journal of Colloid and Interface Science*, 630 (2023) 193-201.

**The publisher's version is available at:**

<https://doi.org/10.1016/j.jcis.2022.10.018>

**When citing, please refer to the published version.**

This full text was downloaded from UNICA IRIS <https://iris.unica.it/>

# The melting curves of calf thymus-DNA are buffer specific

*Monica Mura,<sup>1,2</sup> Cristina Carucci,<sup>1,2</sup> Flaminia Cesare Marincola,<sup>1,2</sup> Maura Monduzzi,<sup>1,2</sup> Drew F.  
Parsons,<sup>1,2\*</sup> Andrea Salis<sup>1,2\*</sup>*

<sup>1</sup>Department of Chemical and Geological Sciences, University of Cagliari, Cittadella Universitaria, SS 554 bivio Sestu, 09042 Monserrato (CA) (Italy).

<sup>2</sup>Consorzio Interuniversitario per lo Sviluppo dei Sistemi a Grande Interfase (CSGI), Florence, Italy, Unità Operativa University of Cagliari, Italy.

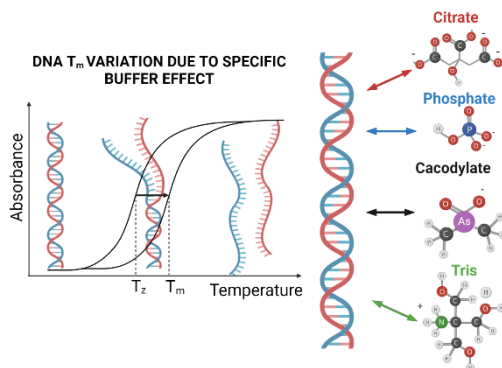
## **Corresponding Authors**

\*email: [asalis@unica.it](mailto:asalis@unica.it) (AS); [drew.parsons@unica.it](mailto:drew.parsons@unica.it) (DFP)

## ABSTRACT

The specific effects of salts (strong electrolytes) on biomolecular properties have been investigated for more than a century. By contrast, the specific role of pH buffers (weak electrolytes and their salts) has usually been ignored. Here, specific buffer effects on DNA thermal stability were evaluated by measuring the melting curve of calf thymus DNA through UV-Vis spectroscopy. The study was carried out using phosphate, Tris, citrate and cacodylate buffers at fixed pH 7.4 with concentration varying systematically in the range 1-600 mM. DNA stability increases with buffer concentration and is influenced specifically by buffer type. To interpret empirical data, a theoretical model was applied with parameters quantifying the impact of buffer on the DNA backbone charge. Comparing the buffer effects via buffer ionic strength rather than buffer concentration, we find DNA is stabilised by buffer in the order Tris > cacodylate > phosphate > citrate.

**KEYWORDS:** Specific buffer effects, DNA, melting temperature, electrostatic interaction.



**Graphical abstract**

## 1. INTRODUCTION

Buffers are important in chemistry and biology for their role in pH regulation. However, it is mostly neglected that buffer species can interact specifically at interfaces [1] in the same way that strong electrolytes are known to do [2–8]. According to the Henderson-Hasselbalch equation [1], the desired pH can be determined solely through the  $pK_a$  and the concentrations of the weak electrolyte and its conjugated acid/base with the buffer species assumed to have no, or minimal, influence on the system [9,10]. Recently, specific buffer effects have emerged in various biochemical systems including enzymes [11,12], proteins [13–16], and nucleotides [17–19]. Previous studies showed that increasing sodium phosphate buffer concentration (0.05 – 1.0 M) increased lysozyme, stem bromelain protease and human serum albumin stability [15]. The thermal stability of lysozyme and hemoglobin decreased along the series TRIS (tris(hydroxymethyl)aminomethane) > TES (*N*-[tris(hydroxymethyl) methyl]-2-aminoethanesulfonic acid) ~ TAPS (*N*-[tris(hydroxymethyl)methyl] 3-aminopropanesulfonic acid) buffer [20]. The diffusion coefficient of monoclonal antibodies was buffer specific, decreasing in the order: citrate > succinate > phosphate > histidine  $\approx$  acetate [21]. It is emerging that, besides controlling pH, buffers species can interact specifically with bio-interfaces, affecting the surface charge [22]. Repulsive and attractive interactions among biomolecules, or between biomolecules and solid surfaces, can thus be modulated either avoiding or favouring aggregation and adsorption [23].

Deoxyribonucleic acid (DNA) is the carrier of genetic information in living organisms as well as a promising molecule in nanotechnology [24], chemical sensing [25] and biomedical applications.<sup>15,16</sup> DNA presents high polymorphism and a variety of

conformations [28] which are affected by hydration and ion interactions [29,30]. DNA stability is strongly influenced by temperature [31], ionic strength [32,33], and pH [34]. Hence, DNA-related experiments require the strict control of pH through the use of buffers [35]. Several studies showed that buffers do affect DNA properties [36–44]. For example, the electrophoretic mobility of DNA, usually considered to be dependent on pH only, was found to decrease in amine-based buffers following the order: tricine (N-tris[hydroxymethyl]methylglycine) > MOPS (3-[N-morpholino]propanesulfonic acid) ~ HEPES (N-[2-hydroxyethyl]piperazine-N'-[2-ethanesulfonic acid]) > TES > BES (N,N-bis[2-hydroxyethyl]-2-aminoethanesulfonic acid) [45]. Another specific buffer effect involving Tris, Bis-Tris propane (BTP), TES, HEPES, and cacodylate was observed in DNA digestion kinetics by EcoRV endonuclease [46]. Recently, changing from Tris to CAPS (3-(cyclohexylamino)propane-1-sulfonic acid) buffers, a better sedimentation of DNA was obtained [35]. Buffer choice needs also to be considered in nucleotide formulation stability [17]. For instance, recently DNA storage was found to be favoured in Tris buffer <sup>15</sup> and used for the formulation of Moderna mRNA COVID-19 vaccines [47], while phosphate buffer was used for Pfizer-BioNTech mRNA COVID-19 vaccines [48].

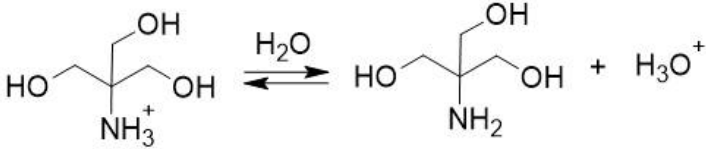
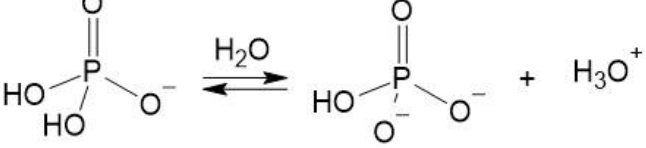
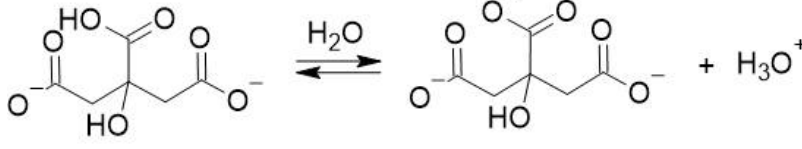
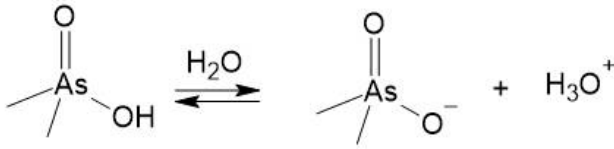
The helical double strand structure of DNA is held together by hydrogen bonds between complementary hydrophobic adenine-thymine (AT) and guanine-cytosine (GC) base pairs, [49] which requires heat to be broken [50]. DNA thermal stability can be evaluated through melting temperatures ( $T_m$ ) [51]: the higher the  $T_m$ , the more thermodynamically stable is the DNA structure [31]. Studies on the effects of electrolytes on DNA thermal stability have shown an increase of  $T_m$  with increasing salt concentration up to 0.5 M, before decreasing at higher concentrations (KBr, (GuH)<sub>2</sub>SO<sub>4</sub>, GuHCl, NaClO<sub>4</sub>) or staying constant (Na<sub>2</sub>SO<sub>4</sub>, KF, KCl, NaCl)

[52]. Typically buffers are used at lower concentrations (5-100 mM, considered negligible) than other electrolytes in the solution [1]. Schildkraut and Lifson were the first to investigate salt concentration effects on DNA stability by measuring the melting temperature of bacterial DNA [53]. In that study, DNA  $T_m$  increased from 78.6 °C in 0.01 M KCl to 98.7 °C in 0.60 M KCl. Melting curves carried out in 150 mM citrate buffer and 450 mM phosphate buffer showed that  $T_m$  increased with increasing buffer concentration [53]. A recent model predicted the  $T_m$  of DNA accounting for the length of the DNA molecule and the content of GC base pairs, but without considering any salt effect [54]. Another model described the process of DNA melting considering a simplified double helix described as a continuum model of two interacting elastic strands [55–57]. By using Poisson-Boltzmann equation coupled with a micromechanical simulation based polyelectrolyte DNA model, it was shown that melting temperature increases with increasing ion concentration [56]. However, a systematic experimental study of the effect of buffer type and concentration on DNA stability has not been reported yet.

Here we studied the specific effect of four buffers commonly used in biochemical systems – namely, Tris-HCl, sodium phosphate, sodium citrate and sodium cacodylate (Table 1) – on the thermal stability of calf thymus DNA at the nominal pH = 7.4. Thermal melting curves were registered through UV-Vis spectroscopy at buffer concentrations ranging from 1 to 100 mM. We introduce a theoretical model to describe and predict the experimental buffer specific dependence of  $T_m$ . The model uses a specific buffer parameter “ $b$ ”, which depends on the average distance between DNA polyion charges in solution, thus quantifying buffer specific interactions. We find that it is important to compare buffers by ionic strength rather than (total) buffer concentration. By combining theory and

experiments, this work demonstrates that buffers (at the same ionic strength) affect DNA thermal stability following the order Tris > cacodylate > phosphate > citrate.

**Table 1.** Buffers used in this work and their  $pK_a$  values at 25°C [58].

Buffer name	Acid/base equilibrium	$pK_a$
<i>Tris</i>		8.06
<i>Phosphate</i>		7.22
<i>Citrate</i>		6.40
<i>Cacodylate</i>		6.30

## 2. EXPERIMENTAL

### 2.1 Chemicals

Sodium citrate dihydrate (99%), citric acid monohydrate (99%), cacodylic acid (98%), monobasic sodium phosphate (99%), disodium hydrogen phosphate (99%), hydrochloric acid (37%), sodium hydroxide (97%), lyophilized calf-thymus DNA were purchased from Sigma Aldrich. Tris(hydroxymethyl)aminomethane (TRIS) was from Bio-Rad.

## 2.2 Preparation of the Buffer solutions and DNA samples

Buffer solutions were prepared by dissolving salts in appropriate volume of distilled water purified through a Millipore system (Simplicity 185). The pH was adjusted at 7.4 with HCl 2 M or NaOH 2 M. The glass electrode was calibrated using a three-points calibration procedure and standard buffer solutions (with nominal pH of 4.00, 7.00, and 9.00). Calf-thymus DNA in concentration 1 mg mL<sup>-1</sup> was dissolved in the different buffer solutions (Tris-HCl, sodium phosphate, sodium cacodylate, or sodium citrate) at 4 °C and gently stirred overnight. Then, the solution was diluted to 25 µg mL<sup>-1</sup> DNA in the same buffer and used for the melting curve determination.

## 2.3 Determination of DNA melting curves through UV-Vis spectroscopy

Double helix DNA thermal melting curves were performed at 260 nm through a Cary 60 UV-Vis spectrophotometer equipped with a thermoelectrically controlled Peltier accessory holding cells of 1 cm path length, magnetically stirring the samples during measurement, and controlling the temperature with an error of  $\pm 0.1$  K. A temperature ramp was made manually over the range 303.0 - 373.0 K, acquiring a data point at every 0.5 K. The quartz cuvette was sealed to avoid sample evaporation. All UV-melting profiles, spectra and difference spectra were measured against a solvent blank. Each melting curve was made in triplicate, and the  $T_m$  value was determined graphically using the following method: linear fits were made over the first and the last parts of the melting curve (before and after degradation where absorbance is stable with no great change in DNA structures); then a median is calculated between the two lines and plotted on the melting profile. The melting temperature  $T_m$  is determined as the point of intersection between the melting curve (in the hyperchromicity region) and the median line [59]. The  $T_m$  average value and standard deviation are reported for each melting experiment.



### 3. EXPERIMENTAL RESULTS

Buffer effects on DNA thermal stability were investigated by determining melting curves through UV-visible spectroscopy. Melting curves were obtained by recording DNA absorbance at 260 nm as a function of temperature. DNA absorbance is due to nitrogen bases that have different UV spectra depending on whether they are coupled (native form) or uncoupled (denatured form). Compared to native DNA, uncoupled bases have a higher absorbance at 260 nm because of the hyperchromic effect [59] due to breaking of hydrogen bonds between complementary nucleobases [60].

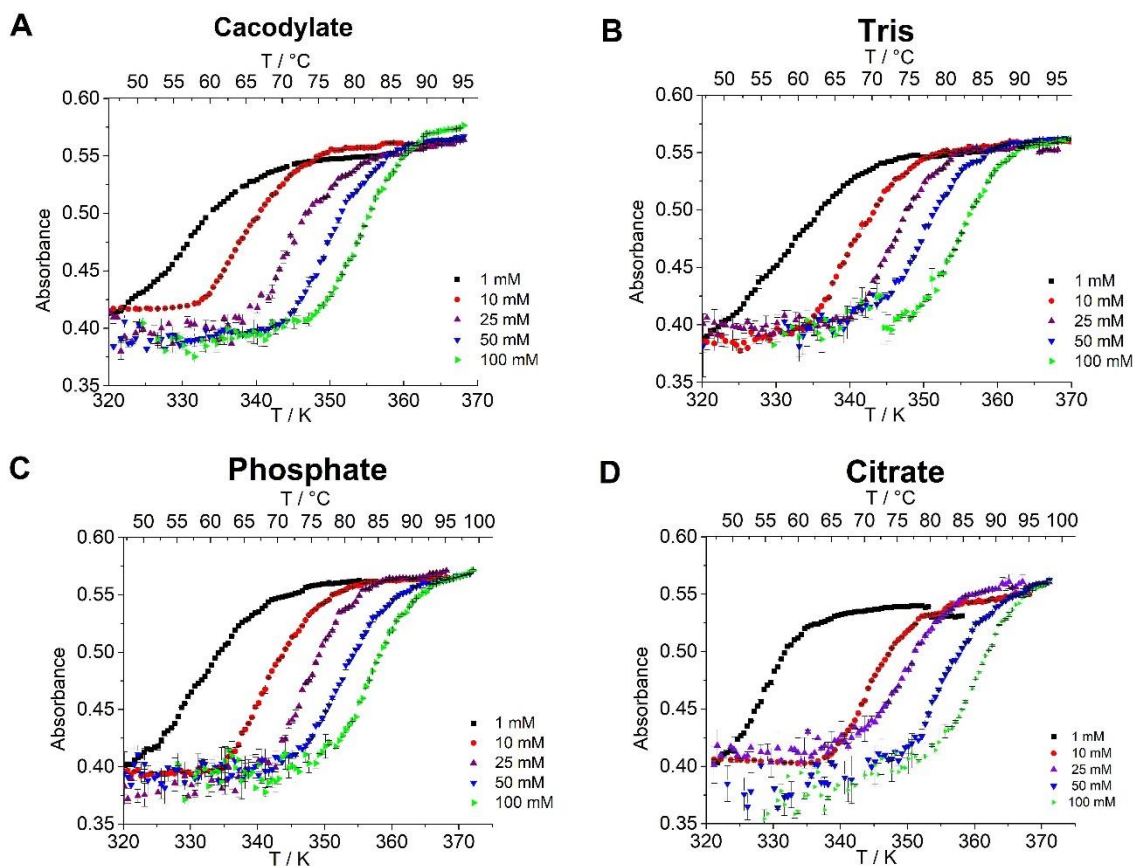


**Fig. 1.** Melting curves at 260 nm for DNA ( $25 \mu\text{g mL}^{-1}$ ) at pH 7.4 in cacodylate (A), Tris (B), phosphate (C) and citrate (D) buffers in the concentration range 1-100 mM.

DNA melting temperature  $T_m$ , defined as the temperature where 50% of the biopolymer is denatured [53], was obtained through a graphical method explained in par. 2.3 and shown in Fig.

S1 (supporting information file).[59] For the sake of comparison,  $T_m$  was also measured in MilliQ water at pH = 7.4 (buffer free), obtaining a value of  $32 \pm 5$  °C ( $305.05 \pm 5$  K). Fig. 1 shows the DNA melting curves measured in cacodylate, Tris, phosphate, and citrate buffers at 5 different concentrations (1, 10, 25, 50 and 100 mM) and at physiological pH (7.4). DNA  $T_m$  values measured in different buffers and at different concentrations are listed in Table S1. All buffers showed the same general behaviour: DNA thermal stability increased as the buffer concentration increased. However,  $T_m$  increased to a different extent depending on the buffer nature, according to the order: cacodylate < Tris < phosphate < citrate (Fig. 2).

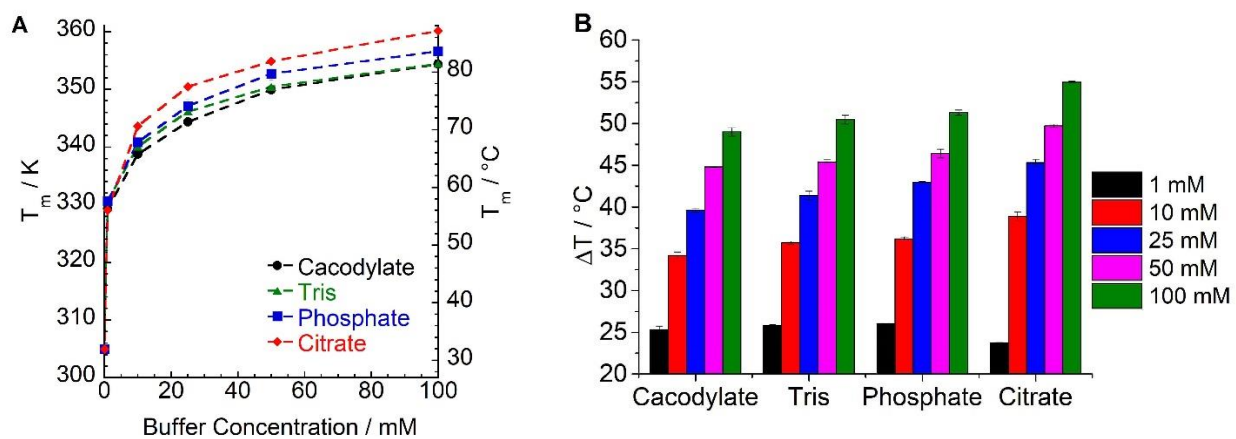


**Fig. 2.** DNA melting temperature dependence on buffer concentration (A) and buffer type (B).

Fig. 2a shows that in MilliQ water (no buffer) the melting temperature of DNA is  $T_m (= T^*) = 32 \pm 5$  °C. Even at very low buffer concentrations (1 mM), DNA stability highly increased, for example, to  $55.7 \pm 0.1$  °C and  $58.0 \pm 0.1$  °C in citrate and phosphate buffers, respectively (Fig. 2a). Compared to the  $T_m$  value measured in MilliQ water (no buffer effect), the variation in the melting temperature ( $\Delta T_m = T_m - T^*$ ) measured at 100 mM buffer concentration was  $\Delta T_m = 48.5$  °C for cacodylate,  $\Delta T_m = 50.0$  °C for Tris-HCl,  $\Delta T_m = 50.8$  °C for phosphate, and  $\Delta T_m = 54.5$  °C for citrate (Fig 2b). Thermal melting curves acquired at buffer concentration 100 mM showed

that  $T_m$  values varied in a range of 81.0 – 87.0 °C (354.1 – 360.1 K) with a difference in  $T_m$  of 6.0 °C between cacodylate and citrate (Fig. S2). Minimal differences in DNA thermal stability (1.7 °C) at 1 mM buffer concentration (Fig.S2a) are found, but at only slightly higher buffer concentrations (10 mM) (Fig. S2b) buffer dependence increased significantly (4.3 °C).

Results in Fig. 2 show that buffer specificity on DNA  $T_m$  increases with increasing buffer concentration. However, the comparison by buffer concentration may be misleading since the effect of buffer solution depends on the specific concentrations of protonated and deprotonated species and thus it is more consistently characterised via ionic strength rather than total buffer concentration [61]. Indeed, each buffer solution at the same concentration presents a different ionic strength because of the different charges of conjugated acid/base species (Table 1). Divalent charged phosphate and trivalent charged citrate species have higher ionic strength than monovalent Tris and cacodylate. In addition, cacodylate has a higher ionic strength than Tris since, due to their respective  $pK_a$  values, at pH 7.4 the concentration of the ionic species of the former is higher than that of the latter. Hence, the experimental data would be better characterised by the ionic strength rather than buffer concentration. This prompts us to develop a thermodynamic model to describe specific buffer effects on DNA thermal stability as a function of ionic strength.

#### 4. THEORY OF SPECIFIC BUFFER EFFECTS ON DNA MELTING

We propose a model which treats the melting temperature  $T_m$  as the equilibrium point between two states of DNA in solution: double helix DNA and coil DNA. The transition between the two states requires a specific amount of energy in the form of heat. This energy is affected by medium composition (solvent polarity, pH, ionic strength, salt/buffer type). Here, the solvent (MilliQ water) and pH (= 7.4) are fixed, so buffer type and ionic strength are the only variables. At

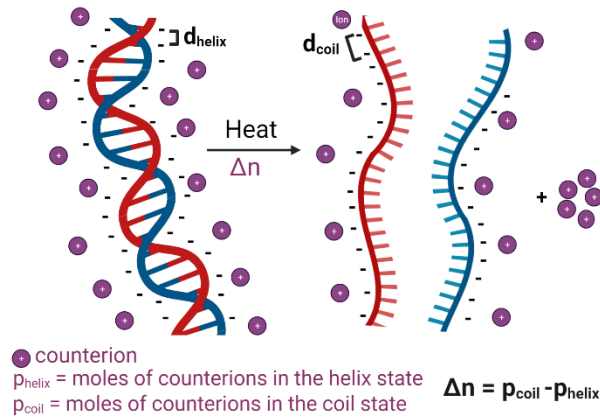
physiological pH and ionic strength (about 150 mM), DNA is a polyelectrolyte whose behavior has been described by Poisson-Boltzmann and counterion-condensation theories [62,63]. DNA charges are shielded by counterions [35], thus limiting its expansion due to repulsive interactions between charged strands [63]. Polyelectrolyte theory provides a good description for the dependence of  $T_m$  on ionic strength [64]. According to the molecular theory of polyelectrolyte solutions [65], the coil-form electrostatic free energy is lower than the helix-form because of a lower charge density. The two states have a different number of counterions locally bound to the phosphate backbones. Following the approach of Rouzina et al [66], the molar free energy difference between helix and coil forms due to the electrolytes ( $\Delta G^{el}$ ) is:

$$\Delta G^{el} = \Delta n k_B T \cdot \ln \left( \frac{I}{I^*} \right) \quad (2)$$

Here,  $k_B$  is the Boltzmann constant,  $T$  the absolute temperature,  $I$  the ionic strength of the electrolyte, and  $I^*$  is the ionic strength of a reference electrolyte. We note that strictly speaking, eq. (2) is only valid in dilute solutions (small  $I$ ). Traditionally [66], the reference state  $I^*$  is taken be the thermodynamic standard state of an ideal solution with ionic strength  $I^* = I^\ominus = 1\text{M}$ , far from a dilute solution. We argue below that it is more constructive to set the reference state using the ionic strength  $I^* = I_0$  of the pure DNA solution without added salt or buffer. For the sake of generality, we present the theory in terms of a general reference state  $I^*$ .  $\Delta n$  is the number of counterions released per DNA phosphate charge during the helix-coil transition [67], because of the difference in linear charge densities of the two states [66]. The release of counterions during melting has been previously demonstrated through osmotic pressure measurements [68].  $\Delta n$  is equal to [66]:

$$\Delta n = p_{coil} - p_{helix} \quad (3)$$

Where  $p_{\text{coil}}$  and  $p_{\text{helix}}$  are the number of counterions per DNA molecule in the coil and double helix state, respectively. The  $p$  value is given by the ratio of the length per unit charge  $d$  of the polyelectrolyte (treated as a cylindrical rod) to the Bjerrum length [66] (the distance at which the interaction energy between two ions in a dielectric medium with dielectric constant  $\epsilon$  equals the thermal energy unit  $k_B T$ .) [69]. That is,  $p$ , defined as the inverse of the conventional linear charge density parameter  $\xi$ , is



**Scheme 1.** DNA backbone charges distance ( $d$ ) in helix and coil form.

$$p = \frac{d \cdot \epsilon_0 \cdot \epsilon \cdot k_B \cdot T}{e^2} \quad (4)$$

where,  $e$  is the elementary charge,  $\epsilon_0$  is the permittivity of the vacuum and  $\epsilon$  is the relative permittivity of water.  $d$  is the average distance between polyion charges (Scheme 1). In general, the transition temperature  $T_m$  is defined as the temperature at which the total change in Gibbs free energy between helix and coil states is zero,  $\Delta G = 0$ . Relative to the reference state with ionic strength  $I^*$ ,  $\Delta G = \Delta G^* + \Delta G^{\text{el}}$ , where  $\Delta G^{\text{el}}$  is the shift in free energy between helix and coil forms due to the electrolyte (Eq.2). At the reference state with ionic strength,  $I^*$ , the melting temperature  $T^*$  is determined by the enthalpy and entropy of the reference state,  $\Delta G^* = 0 = \Delta H^* - T^* \Delta S^*$ . Hence

the reference melting temperature is  $T^* = \Delta H^* / \Delta S^*$ . Away from the reference state, the change in free energy can be expressed in terms of the change in enthalpy and entropy,  $\Delta G = \Delta H - T\Delta S$ . The latter in turn can be described in terms of shifts  $\delta H$  and  $\delta S$  from the reference state,  $\Delta H = \Delta H^* + \delta H$ ,  $\Delta S = \Delta S^* + \delta S$ . With the shift in free energy away from the reference state given by  $\Delta G^{el}$  (Eq.2), the corresponding shifts in enthalpy and entropy are:

$$\delta H = \frac{\partial \Delta G^{el} / T}{\partial (1/T)} \quad \text{and} \quad \delta S = \frac{-\partial \Delta G^{el}}{\partial T} \quad (5)$$

The temperature dependence of  $\Delta G^{el}$  is influenced by the temperature dependence of the permittivity of the solvent, estimated relative to the reference state,

$$\varepsilon(T) = \varepsilon^* \left( \frac{T^*}{T} \right)^\nu \quad (6)$$

A simple estimate of the temperature dependence can be obtained with exponent  $\nu = 1$ , but experimental measurement shows [66] a better description of the temperature dependence is given by  $\nu = 1.4$ . With the shift in free energy given by Eq.2, the shifts in enthalpy and entropy can then estimate as:

$$\delta H = (\nu - 1)\Delta G^{el} \quad (7)$$

$$T\delta S = -(2 - \nu)\Delta G^{el} \quad (8)$$

The equilibrium condition  $\Delta G = 0$ , determining the melting temperature  $T_m$  at a given ionic strength  $I$ , can then be written in terms of  $\Delta G^{el}$  and the change in entropy  $\Delta S^*$  of the reference state. Substituting equations (7) and (8) into Eq. (9), enthalpy-entropy compensation [70] eliminates the dependency on the temperature exponent  $\nu$ :

$$0 = (T^* - T_m) \cdot \Delta S^* + \delta H - T_m \delta S = (T^* - T_m) \cdot \Delta S^* + T_m \Delta G^{el} \quad (9)$$

Finally, applying the polyelectrolyte electrostatic energy from Eq. (2) we obtain a nonlinear formula relating melting temperature to ionic strength:

$$T_m = \frac{T^*}{1 - b \ln(I/I^*)} \quad (10)$$

where we have defined a dimensionless "buffer coefficient"  $b$ ,

$$b = \frac{k_b \Delta n}{\Delta S^*} \quad (11)$$

However, the expression in eq. (2) is a relatively crude estimate of the shift in total free energy due to the electrolyte, not justifying the full nonlinearity in eq. (10). For instance, Rouzina et al. [66] addressed the question of further effects related to heat capacity that go beyond the simple models of eq. (2) and eq. (6). For our purposes, then, it is more convenient to simplify the formula to an expression linear in  $\ln(I/I^*)$  (using the series expansion  $1/(1-x) = 1+x+x^2+\dots \approx 1+x$ , for small  $x$ ), modelling the dependence of the melting temperature on the ionic strength of the electrolyte as:

$$T_m = T^* \left[ 1 + b \cdot \ln \left( \frac{I}{I^*} \right) \right] \quad (12)$$

This simplification assumes that either  $b$  is small ( $b \ll \ln(I/I^*)$ ), or that  $I$  is close to  $I^*$ . The assumption of small  $b$  in the derivation of this formula is equivalent to a small change  $\Delta n$  in DNA charge between the helix and coil states. Ostensibly the formula in Eq.12 fails in the case of no salt in the aqueous medium ( $I=0$ ). But even in pure water there remains a nonzero ionic strength due to self-ionisation of water. More relevantly, we are interested in the case of buffer solution added to a solution of pure DNA. We argue below that  $I_0$ , the ionic strength of the pure DNA solution (including DNA counterions  $\text{Na}^+$ ), defines a suitable reference state ( $I^*=I_0$ ).

## 5. THEORETICAL RESULTS

With a DNA concentration of  $25 \mu\text{g mL}^{-1}$ , the corresponding "zero reference" of the fluid *between* DNA molecules (without added buffer) has ionic strength  $3.5 \times 10^{-5} \text{ M}$ , accounting for  $\text{Na}^+$  (6% in weight of DNA according to the supplier), and  $\text{OH}^-$  and  $\text{H}^+$  at pH 7.4. Once the charge of the DNA phosphate backbone is included (counting bases independently), the ionic strength of the pure DNA solution is determined as  $I_0 = 5.5 \times 10^{-5} \text{ M}$  (with  $120 \mu\text{M}$  bases each with charge density of  $-0.58$  charge/base). The DNA base charge density was calculated as the ratio of DNA negative charges (determined by counterions) to the concentration of bases:

$$\text{base charge density} = \frac{[\text{OH}^-] - [\text{Na}^+] - [\text{H}^+]}{[\text{base}]} \quad (13)$$

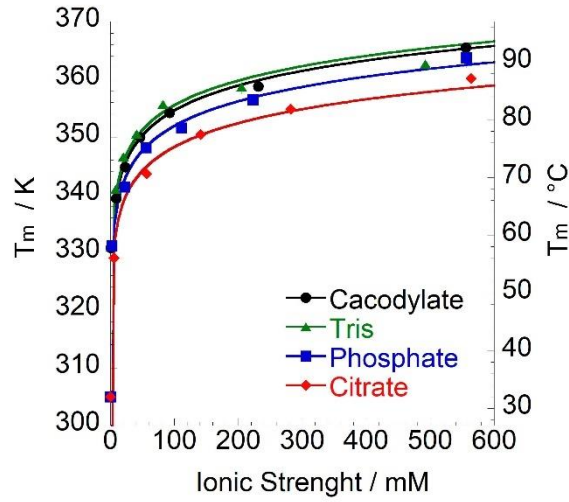


**Fig. 3.** DNA melting temperatures dependent on ionic strength trend fitted through eq. (12).

In the buffer solutions,  $\text{Na}^+$  is present as counterion in solution in different molar ratios balancing anionic buffer charges. To consider the effect of different  $\text{Na}^+$  concentrations on DNA stability,  $T_m$  was reported as a function of ionic strength (Fig. 3). The ionic strength of citrate buffer with 0.1M buffer concentration shown in Fig. 2 ( $T_m$  vs buffer concentration) is 600 mM. We therefore carried out additional experiments to expand the range of ionic strength to 600 mM for each buffer.



Solid lines in Fig. 3 represent the fitting of experimental results obtained through the model developed in the previous section. eq. (12) fits the experimental data well ( $R^2 \geq 0.99$ ). DNA thermal stability follows the order citrate < phosphate < cacodylate < Tris. It is important to note that the series identified here by ionic strength shows a different order to that identified simply by buffer concentration. We expect that  $\text{TrisH}^+$  might have lower interaction with negatively charged DNA than  $\text{Na}^+$  counterions of phosphate and citrate because of steric hindrance. Non-electrostatic interactions also play an important role promoting buffer specificity [61]. Indeed, electrostatic interactions cannot explain alone the experimental dependence of melting temperature on ionic strength (including buffer) shown in Fig. 3. All buffer solutions tend to the same zero-buffer melting temperature  $T_0$  in the limit  $I \rightarrow I_0$  (the zero-buffer concentration limit). Superficially, if we were to use the standard thermodynamic reference of an ideal solution with  $I^* = I^\ominus = 1$  M, each buffer solution individually could be fitted well to eq. (12), with a buffer-specific parameter  $b$ . But the fit would also require a buffer-specific reference temperature  $T^* = T^\ominus$  as shown in Supporting Information Fig. S3, contradicting the requirement that  $T^*$  be a single reference temperature. A simultaneous fit of buffer-specific parameters  $b$  over all buffer solutions with  $I^* = I^\ominus = 1$  M, imposing a common fitted value for  $T^*$ , fits the data poorly (see Fig. S4). The main reason for the discrepancy is that the standard state  $I^\ominus = 1$  M refers to an ideal solution. Alignment with real measurements would require determination of nonideal activity coefficients of all species – DNA, hydronium, buffer ions, counterions – which is not practical for the complex electrolyte considered here.

Instead, it is more constructive to adopt the ionic strength of the pure DNA solution as reference, with  $I^* = I_0 = 5.5 \times 10^{-5}$  M. At this relatively dilute ionic strength, the impact of nonideal activity coefficients is less significant and use of eq. (2) is better justified. More practically, the reference

temperature  $T^*$  then takes on the natural meaning of  $T_0$ , the common melting temperature of DNA in the limit of no added buffer (or salt). Eq. (12) (with  $I^* = I_0 = 5.5 \times 10^{-5}$  M) was used to fit the melting temperature with respect to the ionic strength of buffer solutions reported in Fig. 3. A simultaneous fit was performed over all buffers, determining buffer-specific parameters  $b$  with a common zero-buffer temperature, fitted to  $T_0 = 303.8 \pm 0.4$  K. We note however that even if each buffer solution is fitted separately, similar results are obtained (with  $T_0$  fitted over the range 302-309 K across the 4 buffers considered here), underlining the robustness of the model taking the pure DNA solution as reference. In particular, the fitted value of  $T_0$  agrees excellently with the experimental  $T_m$  measured in MilliQ water,  $305 \pm 5$  K.

## 6. DISCUSSION

The increase of  $T_m$  with increasing buffer concentration can be explained considering that at low buffer concentration a high repulsive interaction between DNA strands occurs. Hence, a low thermal energy to separate the strands is required [53]. Thermal stability increases as a result of buffer specific screening of electrostatic repulsion between DNA strands. Here, we estimated buffer specificity by mean of the buffer coefficient  $b$  obtained from fitting (eq. (12)) and reported in Table S2. Remembering that  $b = k_b \Delta n / \Delta S^0$ , since  $\Delta S^0$  is a property of the pure DNA reference and, as such, is constant in each buffer, the buffer specificity lies in the number of counterions released per DNA phosphate charges  $\Delta n$  during the melting process.  $\Delta n$  is the difference between the average distance between polyion charges at coil ( $d_{\text{coil}}$ ) and helix ( $d_{\text{helix}}$ ) states as indicated in eq. (3). Since  $\Delta n$  is a positive number, we infer that  $d_{\text{coil}} > d_{\text{helix}}$  [71].

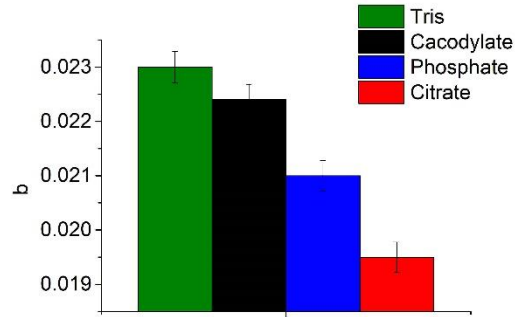


**Fig. 4.** Specific buffer coefficients  $b$

The buffer coefficient  $b$  increases in the order citrate < phosphate < cacodylate < Tris, which corresponds to the DNA stabilization order when measured by ionic strength.  $\Delta n$  (eq. 11) is low when there is not a large difference between the two extreme states. This is satisfied when  $d_{\text{coil}}$  decreases or  $d_{\text{helix}}$  increases. Because single coil DNA is less packed than the double helix, it is safe to assume ions have higher accessibility to the coil state giving a bigger contribution to  $\Delta n$ . Negative buffer species adsorbed onto DNA coil increase charge density and decrease  $d_{\text{coil}}$  between backbones charges. When buffer species interact with DNA, its surface charge is modified. With the increase of negative charges (citrate and phosphate), the electrostatic repulsion between the strands is higher than the monovalent negative cacodylate. The positive (Tris) species shields the phosphate backbone, similar to  $\text{Na}^+$  and  $\text{H}^+$  counterions. This aspect influences DNA stability, here discussed in terms of thermal denaturation. The fitting carried out simultaneously for the four buffers data set gives an accurate value of  $T_0 = 303.8 \pm 0.4$  K, agreeing with the  $T_m = 32 \pm 5$  °C ( $305 \pm 5$  K) experimentally found through DNA melting curves carried out in milliQ water. The standard deviation is largely due to experimentally extreme condition (temperature ramping of melting curves have large range from 5.0 to 75.0 °C). At low ionic strength (and low buffer concentration) there is only a slight buffer effect. The curves split, showing an increased buffer

effect, at 50 mM ionic strength, following the series citrate (trivalent anion) < phosphate (bivalent anion) < cacodylate (monovalent anion) < Tris (monovalent cation). Tris buffer induces the higher DNA stabilisation. Among buffers, Tris, HEPES and phosphate play an important role in gene pharmaceutical formulation, like development of mRNA COVID-19 vaccines.[47,48] DNA electrophoretic mobility measured in Tris-acetate-EDTA (TAE) and Tris-borate-EDTA (TBE) buffers changed from  $3.75 \times 10^{-4} \text{ cm}^2 \text{ V}^{-1} \text{ s}^{-1}$  to  $4.5 \times 10^{-4} \text{ cm}^2 \text{ V}^{-1} \text{ s}^{-1}$  suggesting a DNA-buffer interaction [18]. A study on amine-based buffer effects on DNA cleavage [46] suggested an ion size role influencing the effective interaction by increasing the distance between DNA phosphate groups and buffer species. Larger cations are less effective counterions shielding the charge on DNA phosphate residues than small cations [45]. However, even at the same ionic strength of solutions with  $\text{Na}^+$  as buffer counterion, the DNA stability is different, indicating a specific buffer effect. We recently developed a theoretical model to explain how buffer-specific effects arise from non-electrostatic dispersion forces of the buffer ions [61]. The model described the buffer specific effects on protein zeta potential measurements, and highlighted strong buffer specificity even at low ionic strength. This work shows specific buffer effect on DNA melting temperature even at low ionic strength. Furthermore, for lysozyme, zeta potential values follow a series Tris > cacodylate > phosphate > citrate [61] which corresponds to the DNA thermal stability trend found here.

## CONCLUSIONS

In summary, the present study illustrates how specific buffer effects play a main role on DNA stability. We have observed, through UV-visible melting curves, that DNA stability is buffer type- and concentration-dependent. This confirms the trend observed in previous studies on proteins.

We find that buffer concentration may provide a misleading representation of the buffer effect and recommend using ionic strength to compare buffer solutions. The buffer series identified by ionic strength (Tris > cacodylate > phosphate > citrate) conforms with a theoretical model which correlates buffer specificity not only to species valency, salt concentration and electrostatic interactions, but also to ionic dispersion forces [61]. Our work corroborates specific-buffer effects found in other biopolymers, validating the view that the buffer effect can no longer be neglected. Indeed, significant buffer effects were found even at low buffer concentrations (10 mM). Rouzina et al. model studied DNA melting temperatures at conditions where the ionic strength was high enough to completely screen the negatively charged DNA phosphate backbones. Here we have adapted their model to a system where ionic strength is low, approaching that of the pure DNA solution, close to zero. The theoretical model fits experimental data successfully, fitting each melting curve as function of ionic strength, to obtain a common melting temperature of  $303.8 \pm 0.4$  K for the zero-buffer system. The specific buffer type remains relevant at low ionic strength (50 mM). Furthermore, a buffer coefficient  $b$  is established which quantifies the specific buffer effect with respect to the charge density of DNA.

### **Acknowledgements**

Financial supports from FDS (FdS,F72F20000230007) and Regione Sardegna L.R.7 (CUP: J81G17000150002 and CRP:RASSR79857) are gratefully acknowledged. C.C. thanks MIUR (PON-AIM Azione I.2–DD n. 407-27.02.2018, AIM1890410-2) for fundings.

### **Author contributions**

The manuscript was written through contributions of all authors. All authors have given approval to the final version of the manuscript.

## References

- [1] A. Salis, M. Monduzzi, Not only pH. Specific buffer effects in biological systems, *Curr. Opin. Colloid Interface Sci.* 23 (2016) 1–9. <https://doi.org/10.1016/j.cocis.2016.04.004>.
- [2] K.P. Gregory, G.R. Elliott, H. Robertson, A. Kumar, E.J. Wanless, G.B. Webber, V.S.J. Craig, G.G. Andersson, A.J. Page, Understanding specific ion effects and the Hofmeister series, *Phys. Chem. Chem. Phys.* 24 (2022) 12682–12718. <https://doi.org/10.1039/d2cp00847e>.
- [3] K.P. Gregory, E.J. Wanless, G.B. Webber, V.S.J. Craig, A.J. Page, The electrostatic origins of specific ion effects: Quantifying the Hofmeister series for anions, *Chem. Sci.* 12 (2021) 15007–15015. <https://doi.org/10.1039/d1sc03568a>.
- [4] P. Lo Nostro, B.W. Ninham, Hofmeister Phenomena: An Update on Ion Specificity in Biology, *Chem. Rev.* 112 (2012) 2286–2322. <https://doi.org/10.1021/cr200271j>.
- [5] A. Salis, B.W. Ninham, Models and mechanisms of Hofmeister effects in electrolyte solutions, and colloid and protein systems revisited, *Chem. Soc. Rev.* 43 (2014) 7358–7377. <https://doi.org/10.1039/C4CS00144C>.
- [6] C. Carucci, F. Raccis, A. Salis, E. Magner, Specific ion effects on the enzymatic activity of alcohol dehydrogenase from *Saccharomyces cerevisiae*, *Phys. Chem. Chem. Phys.* 22 (2020) 6749–6754. <https://doi.org/10.1039/C9CP06800G>.
- [7] C. Carucci, A. Salis, E. Magner, Electrolyte effects on enzyme electrochemistry, *Curr. Opin. Electrochem.* 5 (2017) 158–164. <https://doi.org/10.1016/j.coelec.2017.08.011>.
- [8] C. Carucci, A. Salis, E. Magner, Specific Ion Effects on the Mediated Oxidation of NADH, *ChemElectroChem.* 4 (2017) 3075–3080. <https://doi.org/10.1002/celc.201700672>.
- [9] N.E. Good, G.D. Winget, W. Winter, T.N. Connolly, S. Izawa, R.M. Singh, Hydrogen Ion

- Buffers for Biological Research, *Biochemistry*. 5 (1966) 467–477.  
<https://doi.org/10.1021/bi00866a011>.
- [10] G.J. Pielak, Buffers, Especially the Good Kind, *Biochemistry*. 60 (2021) 3436–3440.  
<https://doi.org/10.1021/acs.biochem.1c00200>.
- [11] A. Salis, D. Bilaničová, B.W. Ninham, M. Monduzzi, Hofmeister Effects in Enzymatic Activity: Weak and Strong Electrolyte Influences on the Activity of *Candida rugosa* Lipase, *J. Phys. Chem. B*. 111 (2007) 1149–1156. <https://doi.org/10.1021/jp066346z>.
- [12] H.-K. Kim, E. Tuite, B. Nordén, B.W. Ninham, Co-ion dependence of DNA nuclease activity suggests hydrophobic cavitation as a potential source of activation energy, *Eur. Phys. J. E*. 4 (2001) 411–417. <https://doi.org/10.1007/s101890170096>.
- [13] O.U. Sydney, S. P.Apte, The Effect of Buffers on Protein Conformational Stability, *Pharm. Technol.* 28 (2004) 86–113.
- [14] S. Brudar, B. Hribar-Lee, Effect of buffer on protein stability in aqueous solutions: A simple protein aggregation model, *J. Phys. Chem. B*. 125 (2021) 2504–2512.  
<https://doi.org/10.1021/acs.jpcc.0c10339>.
- [15] P. Pavani, K. Kumar, A. Rani, P. Venkatesu, M.J. Lee, The influence of sodium phosphate buffer on the stability of various proteins: Insights into protein-buffer interactions, *J. Mol. Liq.* 331 (2021) 115753. <https://doi.org/10.1016/j.molliq.2021.115753>.
- [16] F. Cugia, M. Monduzzi, B.W. Ninham, A. Salis, Interplay of ion specificity, pH and buffers: insights from electrophoretic mobility and pH measurements of lysozyme solutions, *RSC Adv.* 3 (2013) 5882. <https://doi.org/10.1039/c3ra00063j>.
- [17] L. Schoenmaker, D. Witzigmann, J.A. Kulkarni, R. Verbeke, G. Kersten, W. Jiskoot, D.J.A. Crommelin, mRNA-lipid nanoparticle COVID-19 vaccines: Structure and stability, *Int. J.*

- Pharm. 601 (2021) 120586. <https://doi.org/10.1016/j.ijpharm.2021.120586>.
- [18] N.C. Stellwagen, C. Gelfi, P.G. Righetti, The free solution mobility of DNA, *Biopolymers*. 42 (1997) 687–703. [https://doi.org/10.1002/\(SICI\)1097-0282\(199711\)42:6](https://doi.org/10.1002/(SICI)1097-0282(199711)42:6).
- [19] H. Šípová-Jungová, L. Jurgová, E. Hemmerová, J. Homola, Interaction of Tris with DNA molecules and carboxylic groups on self-assembled monolayers of alkanethiols measured with surface plasmon resonance, *Appl. Surf. Sci.* 546 (2021). <https://doi.org/10.1016/j.apsusc.2021.148984>.
- [20] P. Pannuru, B.S. Gupta, J. Cherng, H. Ming, J. Lee, Biomolecular interactions of selected buffers with hemoglobin, *J. Therm. Anal. Calorim.* 142 (2020) 2003–2013. <https://doi.org/10.1007/s10973-020-09947-7>.
- [21] D. Roberts, R. Keeling, M. Tracka, C.F. van der Walle, S. Uddin, J. Warwicker, R. Curtis, Specific Ion and Buffer Effects on Protein–Protein Interactions of a Monoclonal Antibody, *Mol. Pharm.* 12 (2015) 179–193. <https://doi.org/10.1021/mp500533c>.
- [22] A. Salis, L. Cappai, C. Carucci, D.F. Parsons, M. Monduzzi, Specific Buffer Effects on the Intermolecular Interactions among Protein Molecules at Physiological pH, *J. Phys. Chem. Lett.* 11 (2020) 6805–6811. <https://doi.org/10.1021/acs.jpcllett.0c01900>.
- [23] F. Cugia, S. Sedda, F. Pitzalis, D.F. Parsons, M. Monduzzi, A. Salis, Are specific buffer effects the new frontier of Hofmeister phenomena? Insights from lysozyme adsorption on ordered mesoporous silica, *RSC Adv.* 6 (2016) 94617–94621. <https://doi.org/10.1039/C6RA17356J>.
- [24] A. Keller, V. Linko, Challenges and Perspectives of DNA Nanostructures in Biomedicine, *Angew. Chemie Int. Ed.* 59 (2020) 15818–15833. <https://doi.org/10.1002/anie.201916390>.
- [25] M.U. Ahmed, S. Nahar, M. Safavieh, M. Zourob, Real-time electrochemical detection of



- pathogen DNA using electrostatic interaction of a redox probe, *Analyst*. 138 (2013) 907–915. <https://doi.org/10.1039/c2an36153a>.
- [26] D. Mathew, S. Sujatha, Interactions of porphyrins with DNA: A review focusing recent advances in chemical modifications on porphyrins as artificial nucleases, *J. Inorg. Biochem.* 219 (2021) 111434. <https://doi.org/10.1016/j.jinorgbio.2021.111434>.
- [27] D. Yang, M.R. Hartman, T.L. Derrien, S. Hamada, D. An, K.G. Yancey, R. Cheng, M. Ma, D. Luo, DNA Materials: Bridging Nanotechnology and Biotechnology, *Acc. Chem. Res.* 47 (2014) 1902–1911. <https://doi.org/10.1021/ar5001082>.
- [28] M. Bansal, DNA Structure: Yet Another Avatar?, *Curr. Sci.* 76 (1999) 1178–1181.
- [29] M. Egli, DNA-Cation Interactions, *Chem. Biol.* 9 (2002) 277–286. [https://doi.org/10.1016/S1074-5521\(02\)00116-3](https://doi.org/10.1016/S1074-5521(02)00116-3).
- [30] W. Zhou, R. Saran, J. Liu, Metal Sensing by DNA, *Chem. Rev.* 117 (2017) 8272–8325. <https://doi.org/10.1021/acs.chemrev.7b00063>.
- [31] R.D. Blake, S.G. Delcourt, Thermal stability of DNA, *Nucleic Acids Res.* 26 (1998) 3323–3332. <https://doi.org/10.1093/nar/26.14.3323>.
- [32] B. Gao, X.-M. Hou, Opposite Effects of Potassium Ions on the Thermal Stability of i-Motif DNA in Different Buffer Systems, *ACS Omega.* 6 (2021) 8976–8985. <https://doi.org/10.1021/acsomega.0c06350>.
- [33] P. Doty, H. Boedtker, J.R. Fresco, R. Haselkorn, M. Litt, Secondary structure in ribonucleic acids, *Proc. Natl. Acad. Sci.* 45 (1959) 482–499. <https://doi.org/10.1073/pnas.45.4.482>.
- [34] R. Owczarzy, B.G. Moreira, Y. You, M.A. Behlke, J.A. Walder, Predicting Stability of DNA Duplexes in Solutions Containing Magnesium and Monovalent Cations, *Biochemistry.* 47 (2008) 5336–5353. <https://doi.org/10.1021/bi702363u>.

- [35] M. Schenkelberger, C. Trapp, T. Mai, V. Giri, M. Mohammadi-Kambs, A. Ott, Ultrahigh molecular recognition specificity of competing DNA oligonucleotide strands in thermal equilibrium: a cooperative transition to order, *New J. Phys.* 23 (2021) 043044. <https://doi.org/10.1088/1367-2630/abecb0>.
- [36] G. Zhang, X. Hu, N. Zhao, W. Li, L. He, Studies on the interaction of aminocarb with calf thymus DNA by spectroscopic methods, *Pestic. Biochem. Physiol.* 98 (2010) 206–212. <https://doi.org/10.1016/j.pestbp.2010.06.008>.
- [37] G. Zhang, Y. Ma, Spectroscopic studies on the interaction of sodium benzoate, a food preservative, with calf thymus DNA, *Food Chem.* 141 (2013) 41–47. <https://doi.org/10.1016/j.foodchem.2013.02.122>.
- [38] G. Zhang, X. Hu, J. Pan, Spectroscopic studies of the interaction between pirimicarb and calf thymus DNA, *Spectrochim. Acta Part A Mol. Biomol. Spectrosc.* 78 (2011) 687–694. <https://doi.org/10.1016/j.saa.2010.11.050>.
- [39] G. Zhang, P. Fu, L. Wang, M. Hu, Molecular Spectroscopic Studies of Ferrerol Interaction with Calf Thymus DNA, *J. Agric. Food Chem.* 59 (2011) 8944–8952. <https://doi.org/10.1021/jf2019006>.
- [40] F. Cui, R. Huo, G. Hui, X. Lv, J. Jin, G. Zhang, W. Xing, Study on the interaction between aglycon of daunorubicin and calf thymus DNA by spectroscopy, *J. Mol. Struct.* 1001 (2011) 104–110. <https://doi.org/10.1016/j.molstruc.2011.06.024>.
- [41] A. Ahmad, M. Ahmad, Deciphering the mechanism of interaction of edifenphos with calf thymus DNA, *Spectrochim. Acta Part A Mol. Biomol. Spectrosc.* 188 (2018) 244–251. <https://doi.org/10.1016/j.saa.2017.07.014>.
- [42] L. Messori, P. Orioli, C. Tempi, G. Marcon, Interactions of Selected Gold(III) Complexes

- with Calf Thymus DNA, *Biochem. Biophys. Res. Commun.* 281 (2001) 352–360.  
<https://doi.org/10.1006/bbrc.2001.4358>.
- [43] A.H. Hegde, S.N. Prashanth, J. Seetharamappa, Interaction of antioxidant flavonoids with calf thymus DNA analyzed by spectroscopic and electrochemical methods, *J. Pharm. Biomed. Anal.* 63 (2012) 40–46. <https://doi.org/10.1016/j.jpba.2012.01.034>.
- [44] N.C. Stellwagen, C. Gelfi, P.G. Righetti, DNA and buffers: The hidden danger of complex formation, *Biopolymers.* 54 (2000) 137–142. [https://doi.org/10.1002/1097-0282\(200008\)54:2](https://doi.org/10.1002/1097-0282(200008)54:2).
- [45] N.C. Stellwagen, A. Bossi, C. Gelfi, P.G. Righetti, DNA and Buffers: Are There Any Noninteracting, Neutral pH Buffers?, *Anal. Biochem.* 287 (2000) 167–175.  
<https://doi.org/10.1006/abio.2000.4848>.
- [46] J.R. Wenner, V.A. Bloomfield, Buffer Effects on EcoRV Kinetics as Measured by Fluorescent Staining and Digital Imaging of Plasmid Cleavage, *Anal. Biochem.* 268 (1999) 201–212. <https://doi.org/10.1006/abio.1998.3079>.
- [47] European Medicines Agency; Science Medicine Health, Assessment report: COVID-19 mRNA vaccine (nucleoside-modified) Procedure No. EMEA/H/C/005791/0000, 2021.  
<https://doi.org/EMA/15689/2021>.
- [48] European Medicines Agency; Science Medicine Health, Assessment report: COVID-19 mRNA vaccine (nucleoside-modified) Procedure No. EMEA/H/C/005735/0000, 2021.  
<https://doi.org/EMA/707383/2020>.
- [49] M. Bansal, DNA structure: Revisiting the Watson–Crick, *Curr. Sci.* 85 (2003) 557.  
<https://www.jstor.org/stable/24110017>.
- [50] S. Hadži, J. Lah, Origin of heat capacity increment in DNA folding: The hydration effect,

- Biochim. Biophys. Acta - Gen. Subj. 1865 (2021) 129774.  
<https://doi.org/10.1016/j.bbagen.2020.129774>.
- [51] A. Vologodskii, M.D. Frank-Kamenetskii, DNA melting and energetics of the double helix, *Phys. Life Rev.* 25 (2018) 1–21. <https://doi.org/10.1016/j.plrev.2017.11.012>.
- [52] M.T. Record, E. Guinn, L. Pegram, M. Capp, Introductory Lecture: Interpreting and predicting Hofmeister salt ion and solute effects on biopolymer and model processes using the solute partitioning model, *Faraday Discuss.* 160 (2013) 9–44. <https://doi.org/10.1039/c2fd20128c>.
- [53] C. Schildkraut, S. Lifson, Dependence of the melting temperature of DNA on salt concentration, *Biopolymers.* 3 (1965) 195–208. <https://doi.org/10.1002/bip.360030207>.
- [54] D.A. Belov, Y.V. Belov, I.G. Kiselev, Modeling of the DNA Melting Point Dependence on Various Analysis Factors, in: 2020 Int. Multi-Conference Ind. Eng. Mod. Technol., IEEE, 2020: pp. 1–3. <https://doi.org/10.1109/FarEastCon50210.2020.9271634>.
- [55] M. Moakher, J.H. Maddocks, A Double-Strand Elastic Rod Theory, *Arch. Ration. Mech. Anal.* 177 (2005) 53–91. <https://doi.org/10.1007/s00205-005-0360-y>.
- [56] J. Singh, P.K. Purohit, Statistical mechanics of a double-stranded rod model for DNA melting and elasticity, *Soft Matter.* 16 (2020) 7715–7726. <https://doi.org/10.1039/D0SM00521E>.
- [57] J. Singh, P.K. Purohit, Allosteric interactions in a birod model of DNA, *Proc. R. Soc. A Math. Phys. Eng. Sci.* 474 (2018). <https://doi.org/10.1098/rspa.2018.0136>.
- [58] V.S. Stoll, J.S. Blanchard, Buffers: Principles and Practice, in: *Methods Enzymol.*, 2009: pp. 43–56. [https://doi.org/10.1016/S0076-6879\(09\)63006-8](https://doi.org/10.1016/S0076-6879(09)63006-8).
- [59] J.-L. Mergny, L. Lacroix, Analysis of Thermal Melting Curves, *Oligonucleotides.* 13 (2003)

- 515–537. <https://doi.org/10.1089/154545703322860825>.
- [60] D. Freifelder, P.F. Davison, Hyperchromicity and Strand Separation in Bacterial DNA, *Biophys. J.* 2 (1962) 249–256. [https://doi.org/10.1016/S0006-3495\(62\)86853-2](https://doi.org/10.1016/S0006-3495(62)86853-2).
- [61] D.F. Parsons, C. Carucci, A. Salis, Buffer-specific effects arise from ionic dispersion forces, *Phys. Chem. Chem. Phys.* 24 (2022) 6544–6551. <https://doi.org/10.1039/D2CP00223J>.
- [62] J. Lipfert, S. Doniach, R. Das, D. Herschlag, Understanding Nucleic Acid–Ion Interactions, *Annu. Rev. Biochem.* 83 (2014) 813–841. <https://doi.org/10.1146/annurev-biochem-060409-092720>.
- [63] C.F. Anderson, M.T. Record, Polyelectrolyte Theories and their Applications to DNA, *Annu. Rev. Phys. Chem.* 33 (1982) 191–222. <https://doi.org/10.1146/annurev.pc.33.100182.001203>.
- [64] I. Rouzina, V.A. Bloomfield, Macroion Attraction Due to Electrostatic Correlation between Screening Counterions. 1. Mobile Surface-Adsorbed Ions and Diffuse Ion Cloud, *J. Phys. Chem.* 100 (1996) 9977–9989. <https://doi.org/10.1021/jp960458g>.
- [65] G.S. Manning, The molecular theory of polyelectrolyte solutions with applications to the electrostatic properties of polynucleotides, *Q. Rev. Biophys.* 11 (1978) 179–246. <https://doi.org/10.1017/S0033583500002031>.
- [66] I. Rouzina, V.A. Bloomfield, Heat Capacity Effects on the Melting of DNA. 1. General Aspects, *Biophys. J.* 77 (1999) 3242–3251. [https://doi.org/10.1016/S0006-3495\(99\)77155-9](https://doi.org/10.1016/S0006-3495(99)77155-9).
- [67] R. Owczarzy, Y. You, B.G. Moreira, J.A. Manthey, L. Huang, M.A. Behlke, J.A. Walder, Effects of Sodium Ions on DNA Duplex Oligomers: Improved Predictions of Melting Temperatures, *Biochemistry.* 43 (2004) 3537–3554. <https://doi.org/10.1021/bi034621r>.

- [68] C.H. Spink, J.B. Chaires, Effects of hydration, ion release, and excluded volume on the melting of triplex and duplex DNA, *Biochemistry*. 38 (1999) 496–508. <https://doi.org/10.1021/bi9820154>.
- [69] A.A. Lee, C.S. Perez-Martinez, A.M. Smith, S. Perkin, Scaling Analysis of the Screening Length in Concentrated Electrolytes, *Phys. Rev. Lett.* 119 (2017) 1–5. <https://doi.org/10.1103/PhysRevLett.119.026002>.
- [70] J. Petruska, M.F. Goodman, Enthalpy-entropy compensation in DNA melting thermodynamics, *J. Biol. Chem.* 270 (1995) 746–750. <https://doi.org/10.1074/jbc.270.2.746>.
- [71] M.C. Williams, J.R. Wenner, I. Rouzina, V.A. Bloomfield, Entropy and Heat Capacity of DNA Melting from Temperature Dependence of Single Molecule Stretching, *Biophys. J.* 80 (2001) 1932–1939. [https://doi.org/10.1016/S0006-3495\(01\)76163-2](https://doi.org/10.1016/S0006-3495(01)76163-2).